Energy Storage Materials 76 (2025) 104149

Contents lists available at ScienceDirect

Energy Storage Materials

journal homepage: www.elsevier.com/locate/ensm

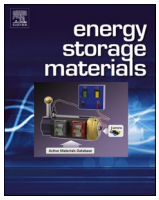

Innovating high-performance aqueous sodium-ion batteries with ice-resistant inorganic electrolytes for -40 °C applications

Gengzheng liu [a], Huilian Hao [a,*], Zefei Guo [a], Jun Yang [a], Wenzhong Shen [b,*]

[a] School of Materials Science and Engineering, Shanghai University of Engineering Science, Shanghai, 201620, China
[b] Institute of Solar Energy, and Key Laboratory of Artificial Structures and Quantum Control (Ministry of Education), School of Physics and Astronomy, Shanghai Jiao Tong University, Shanghai, 200240, China

ARTICLE INFO

Keywords:
Aqueous sodium-ion batteries
Low-temperature
Long cycle life
High ionic conductivity
Magnesium chloride hexahydrate

ABSTRACT

Aqueous sodium-ion batteries (ASIBs) are increasingly recognized for their high safety, eco-friendliness, and cost advantages. However, the high freezing point of aqueous electrolytes significantly limits their practical applications in low-temperature environments. To address this challenge, this study introduces an innovative 0.5 M NaCl + 2.8 M $MgCl_2{\cdot}6H_2O$ electrolyte, effectively lowering the freezing point to -50 °C. The strong interaction between Mg^{2+} and water molecules disrupts the hydrogen bonding network in water. As a result, the optimized electrolyte exhibits an impressive ionic conductivity of 9.36 mS cm^{-1} even at -50 °C. Using $Na_2CoFe(CN)_6$ as the cathode and activated carbon as the anode materials for ASIBs, the system achieved an excellent discharge capacity of 74.0 mAh g^{-1} at -40 °C under 1 C (1 C = 150 mA g^{-1}). Even more impressively, the battery showed no capacity degradation after 10,000 cycles at -40 °C and successfully lit an LED bulb at the same temperature. This work not only broadens the applicability of ASIBs but also provides a robust foundation for the development of high-performance, low-temperature energy storage solutions capable of meeting demanding environmental requirements.

1. Introduction

In response to the rapid growth of global renewable energy demand, energy storage technology is pivotal for sustainable development [1–3]. Lithium-ion batteries have attracted widespread attention due to their excellent energy and power density [4–6]. However, compared to lithium resources, sodium resources are abundant in the Earth's crust and more economical, making sodium-ion batteries an appealing option. In large-scale energy storage applications, safety and cost are crucial factors [7–9]. Aqueous sodium-ion batteries (ASIBs) show great promise for development due to their high ionic conductivity, safety, low cost, and environmental benefits, further reinforcing their status as a viable choice [10,11]. Traditional aqueous batteries are susceptible to freezing in low-temperature environments (−20 °C), which restricts ion transport and slows reaction kinetics, thereby severely impacting the overall performance of energy storage systems [12–14]. Furthermore, the relatively low electrochemical window of water (~ 1.23 V) limits its application [15,16]. Therefore, there is an urgent need to improve battery performance in order to expand the operating temperature range and broaden the voltage window, enabling reliable operation across a wider range of environmental conditions.

As a key battery component, electrolyte plays a crucial role in advancing ASIBs performance by directly enhancing ionic conductivity and battery cycle life. In recent years, researchers have achieved notable progress in developing innovative anti-freeze electrolytes [17–26]. One common method to reduce the freezing point of the electrolyte is by introducing organic co-solvents [17–22]. Organic polar solvents with some functional groups have strong coordination ability with water molecules, which reduces the content of free water in the solution and effectively reduces the freezing point of the solution. For example, Rong et al. reported the addition ethylene glycol in the electrolyte, which operated successfully at −40 °C with a conductivity of 2.38 mS cm^{-1} and a capacity retention of 88.3% after 5000 cycles at −20 °C [17]. Zhu et al. reported that adding formamide as a co-solvent and antifreeze into the electrolyte enables 8000 cycles without obvious capacity decay, while achieving an ionic conductivity of 1.75 mS cm^{-1} achieved at −50 °C [18]. Similarly, dimethyl sulfoxide [19], glycerol [20], methanol [21], N,N-Dimethylformamide [22] have also been reported in the field of low-temperature aqueous batteries. However, their high viscosity and polarity can adversely impact ionic conductivity. Additionally, the

* Corresponding authors.
E-mail addresses: sulee8866@126.com (H. Hao), wzshen@sjtu.edu.cn (W. Shen).

https://doi.org/10.1016/j.ensm.2025.104149
Received 6 December 2024; Received in revised form 16 January 2025; Accepted 27 February 2025
Available online 28 February 2025

inherent toxicity of organic solvents undermines the non-toxic advantage of ASIBs, making a shift toward pure inorganic electrolytes a more favorable choice.

Increasing salt concentration is identified as an effective strategy to improve electrolyte performance under low-temperature conditions [23,24]. For instance, Zhang et al. reported using a 17 M $NaClO_4$ electrolyte for ASIBs, achieving ionic conductivity of 4.4 mS cm^{-1} at −40 °C [23]. Zhang et al. reported a battery employing 7.5 M $ZnCl_2$ as the electrolyte with an ionic conductivity reaching 1.79 mS cm^{-1} at −60 °C [24]. These findings demonstrate the effectiveness of high-concentration electrolytes in enhancing battery performance in cold environments. However, high salt concentrations not only reduce electrolyte electrical conductivity but also raise production costs and pose challenges to manufacturing quality, limiting their practicality [25,26]. Zhao et al. reported a low-concentration, purely inorganic electrolyte composed of $MnCl_2{\cdot}4H_2O$/NaCl for ASIBs. This electrolyte demonstrates an ionic conductivity of 2.44 mS cm^{-1} at −50 °C and enables ASIBs to achieve a cycle life of 10,000 cycles at −40 °C, with a capacity retention of 99% [26]. Consequently, developing pure inorganic, low-concentration electrolytes presents a promising alternative to enhance battery performance at low temperatures while maintaining economic and practical feasibility.

In this study, the pure inorganic NaCl/$MgCl_2{\cdot}6H_2O$ electrolyte is used for the first time to lower the freezing point of aqueous electrolytes, providing a cost-effective solution. Due to its strong interactions between Mg^{2+} and water molecule, which can disrupt the original hydrogen bonding network and result in a lower freezing point compared to the single NaCl electrolyte, as illustrated in Fig. 1. At −50 °C, the optimized electrolyte exhibits excellent ionic conductivity (9.36 mS cm^{-1}), even surpassing those of some organic solvents at room temperature. A battery assembled with $Na_2CoFe(CN)_6$ and activated carbon as the cathode and anode, demonstrates a long cycle life and impressive specific capacity at −40 °C, and an LED light can be successfully powered, showcasing the potential of the electrolyte for low-temperature applications. The use of this inert inorganic electrolyte broadens the temperature range for electrolyte applications, providing valuable insights for designing low-temperature aqueous batteries.

2. Results and discussion

The operating schematic diagram of the charging and discharging mechanism for ASIBs is shown in Fig. 2a. Both the electrode and electrolytes are composed of pure inorganic materials. It is well known that when the ambient temperature is close to the freezing point of the electrolyte, the viscosity of the solution increases rapidly, resulting in the significant decrease of the ion transport rate and poor low-temperature performance of the battery [27]. Therefore, lowering the freezing point of the electrolyte and increasing its conductivity are effective strategies to maintain the excellent performance at low temperatures [28]. It is noted that the salt concentration of the solution for the lowest freezing point is referred to the eutectic concentration, which can be intuitively represented by the eutectic phase diagram of binary aqueous systems. According to the binary phase diagram of $MgCl_2{\cdot}6H_2O$ (Fig. S1), it can be seen that the solution has the lowest freezing point when the concentration of $MgCl_2{\cdot}6H_2O$ is 2.8 M (mol L^{-1}) [29]. In addition, 0.5 M NaCl salt is added to provide shuttle ions during cycling. To optimize the electrolyte, 0.5 M NaCl and $MgCl_2{\cdot}6H_2O$ solutions with different concentrations were mixed. The prepared samples are expressed as 0.5 M NaCl+ X M $MgCl_2{\cdot}6H_2O$ ($X = 0, 0.5, 1.0, 1.5, 2.0, 2.8, 3.5$) and were placed at different temperatures (25 °C ~ −50 °C) for 2 h, as depicted in Fig. 2b and Fig. S2. It can be observed that all samples are colorless and transparent at room temperature (25 °C). It can be clearly observed that only 0.5 M NaCl+ 2.8 M $MgCl_2{\cdot}6H_2O$ electrolyte remains liquid even at −50 °C. In addition, the 0.5 M NaCl electrolyte is completely frozen after keeping at −10 °C for 24 h (Fig. S3). It should be noted that, the 0.5 M NaCl + 2.8 M $MgCl_2{\cdot}6H_2O$ electrolyte still remains good fluidity at −50 °C for 30 days (Fig. S4), and freezes completely when the temperature reaches −55 °C, as shown in the Fig. S5. The electrochemical impedance spectroscopy (EIS) tests were performed to calculate the ionic conductivity for 0.5 M NaCl + 2.8 M $MgCl_2{\cdot}6H_2O$ electrolyte and 0.5 M NaCl electrolyte at different temperatures (Fig. S6), and the results are shown in Fig. 2c and Fig. S7, respectively. At room temperature, the ionic conductivity of the 0.5 M NaCl + 2.8 M $MgCl_2{\cdot}6H_2O$ electrolyte reaches 166.09 mS cm^{-1}, which is three times higher than that of 0.5 M NaCl electrolyte. Furthermore, at a temperature of −50 °C, the ionic conductivity of the 0.5 M NaCl + 2.8 M

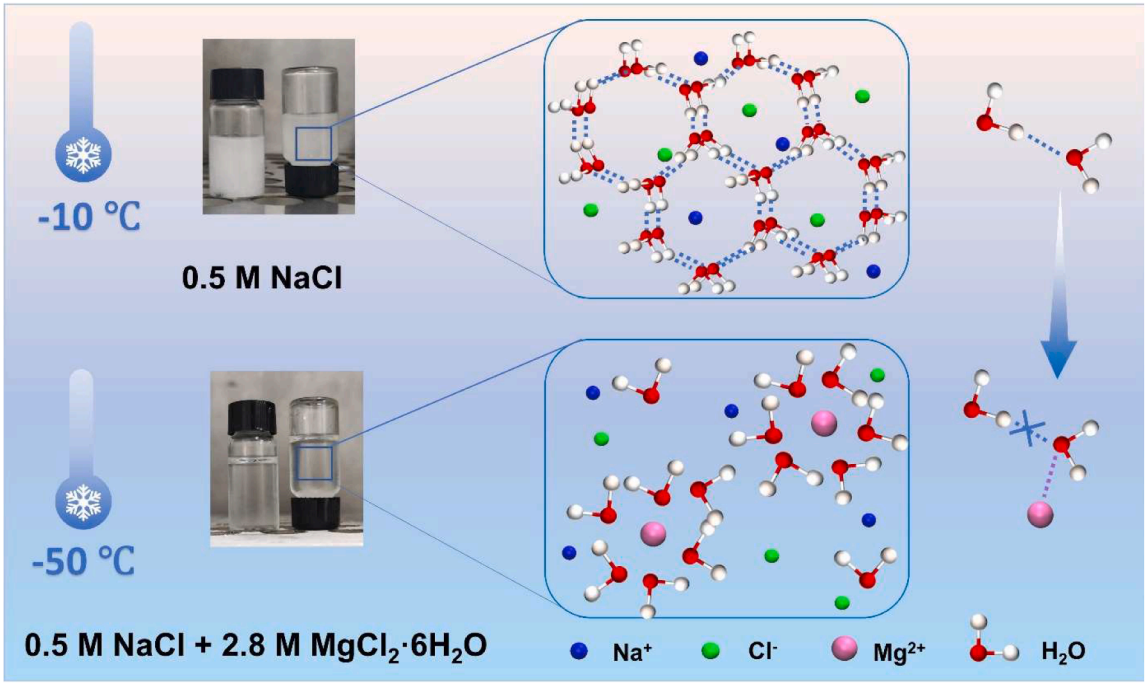

Fig. 1. Schematic diagram of structural evolution of pure inorganic low-temperature electrolytes.

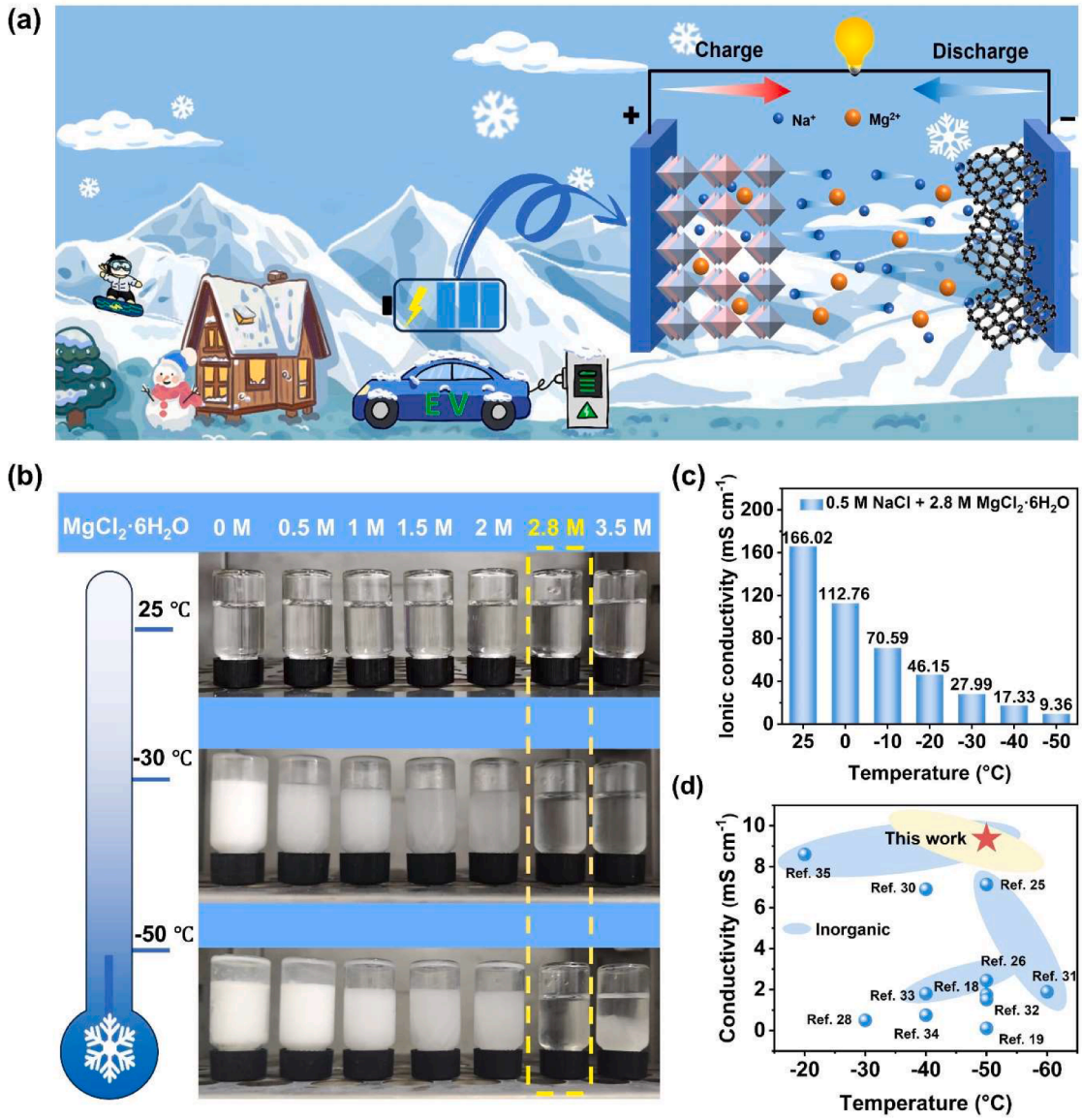

Fig. 2. (a) The operating schematic diagram of the pure inorganic storage system in this work. (b) The optical images of 0.5 M NaCl-based solutions with different concentrations of $MgCl_2{\cdot}6H_2O$ under 25 °C, −30 °C and −50 °C. (c) The ionic conductivity of 0.5 M NaCl + 2.8 M $MgCl_2{\cdot}6H_2O$ electrolyte at different temperatures. (d) The comparison of conductivity between this work and previous reports at different temperatures.

$MgCl_2{\cdot}6H_2O$ electrolyte reach an impressive 9.36 mS cm^{-1}, which is considerably higher than the reported results [18,19,25,26,28,30–35], as plotted in Fig. 2d.

The electrochemical stability window (ESW) is an important parameter for ASIBs, and the narrow ESW (~ 1.23 V) of conventional aqueous electrolytes is a result of the limitation of the water splitting voltage [36]. As shown in Fig. S8, linear sweep voltammetry tests were performed on 0.5 M NaCl, 2.8 M $MgCl_2{\cdot}6H_2O$, and 0.5 M NaCl + 2.8 M $MgCl_2{\cdot}6H_2O$ electrolytes, and the ESW is 2.2 V, 1.96 V, and 2.05 V, respectively, much higher than those of water and the conventional aqueous electrolytes (≤ 2 V) [37,38]. In order to verify the effect of the $MgCl_2{\cdot}6H_2O$ on the freezing point of the NaCl electrolyte, the glass-liquid transition temperatures of different electrolytes were studied by differential scanning calorimetry (DSC), as shown in the Fig. S9. Typically, distinct endothermic peaks are observed during the melting of ice. The DSC curves were obtained by cooling the electrolytes to −150 °C and subsequently heating them to 25 °C at a rate of 5 °C·min^{-1}. The results indicate that the initial glass transition temperature of the optimized electrolyte is −118 °C, with the glass transition temperature range (T_g) spanning from −118 °C to −126 °C.

The freezing point of H_2O is closely related to the number of hydrogen bonds. By introducing metal ions, strong interactions between water molecules and the metal ions can be formed, effectively breaking the original hydrogen bond network in water, and resulting in the decrease of the freezing point of the solution [18,39–41]. To theoretically verify the effect of 2.8 M $MgCl_2{\cdot}6H_2O$ on the freezing point of 0.5 M NaCl electrolyte, molecular dynamics (MD) simulations are used to examine the evolution of hydrogen bonding networks for both the 0.5 M NaCl and 0.5 M NaCl + 2.8 M $MgCl_2{\cdot}6H_2O$ electrolytes, as well as the coordination number between cations and oxygen atoms in 0.5 M NaCl + 2.8 M $MgCl_2{\cdot}6H_2O$ electrolyte. It can be seen from Figs. 3a and 3b, the number of hydrogen bonds between water molecules in 0.5 M NaCl + 2.8 M $MgCl_2{\cdot}6H_2O$ electrolyte (~ 1.20) is significantly less than that of the 0.5 M NaCl electrolyte (~ 1.618), meanwhile a large number of Mg^{2+}···O—H bonds are formed in 0.5 M NaCl + 2.8 M $MgCl_2{\cdot}6H_2O$ electrolyte, results in the significantly decrease of freezing point [26]. This is attributed to the strong interaction between Mg^{2+} and water molecules, which destroys the hydrogen bond network between water

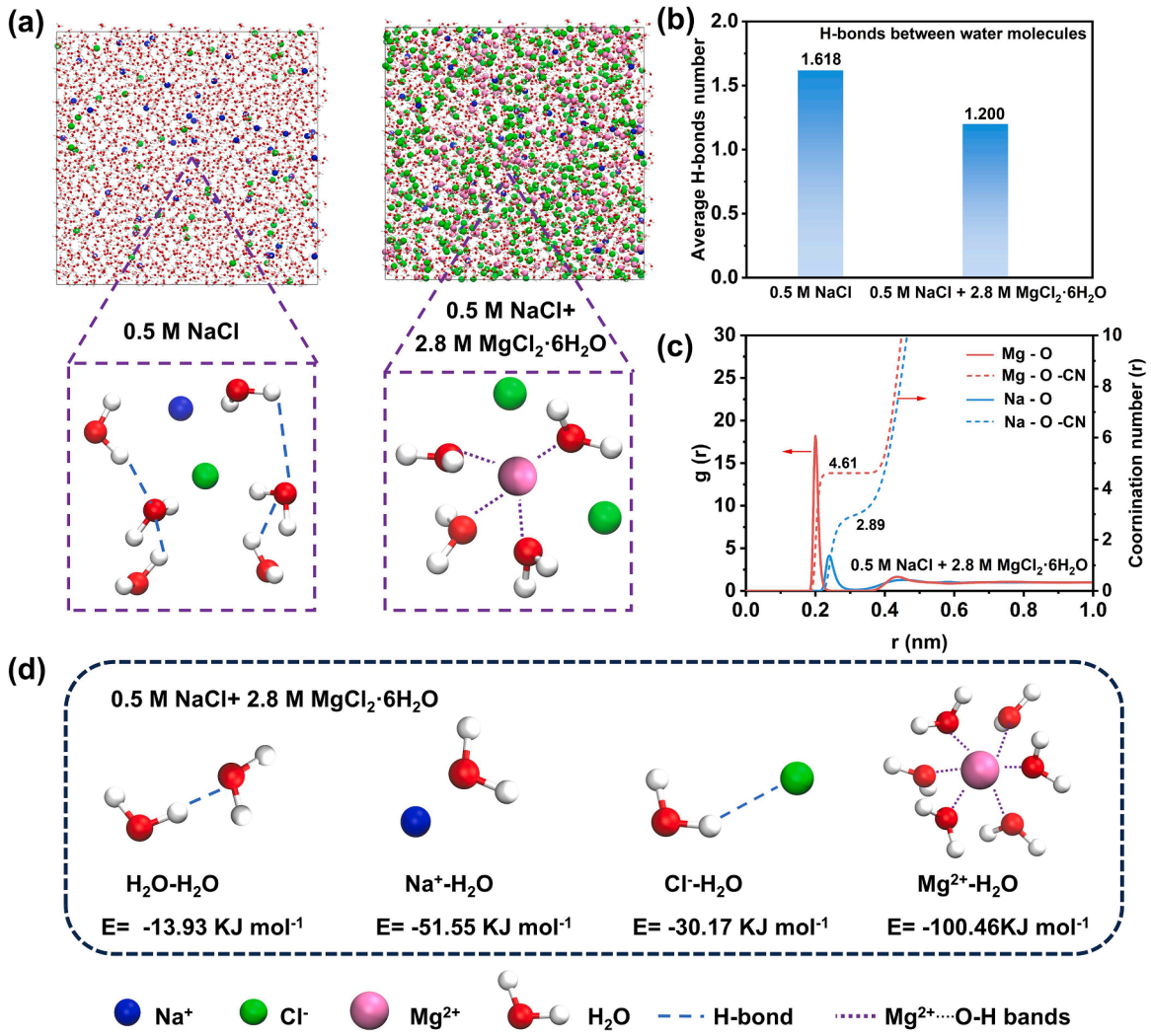

Fig. 3. (a) MD simulation snapshots for 0.5 M NaCl (left) and 0.5 M NaCl + 2.8 M $MgCl_2{\cdot}6H_2O$ (right) electrolytes, respectively. (b) The average number of hydrogen bonds between water molecules for different electrolytes. (c) The radial distribution function of 0.5 M NaCl + 2.8 M $MgCl_2{\cdot}6H_2O$ electrolyte. (d) The interaction energy from DFT calculation for individual H_2O molecule and other particles in 0.5 M NaCl + 2.8 M $MgCl_2{\cdot}6H_2O$ electrolyte.

molecules. By analyzing the radial distribution functions of Mg^{2+} and Na^+ with oxygen atoms in 0.5 M NaCl + 2.8 M $MgCl_2{\cdot}6H_2O$ electrolyte (Fig. 3c), it is determined that Mg^{2+} is coordinated with an average of 4.61 water molecules, whereas Na^+ has a coordination number of 2.89 with water molecules, suggesting that Mg^{2+} plays an important role in lowering the freezing point of solutions. Furthermore, the interaction energies between individual water molecules and other particles in 0.5 M NaCl + 2.8 M $MgCl_2{\cdot}6H_2O$ electrolyte are calculated by density functional theory (DFT) calculation, as illustrated in Fig. 3d. It can be observed that the interaction energies of H_2O—H_2O, Na^+-H_2O, Cl^--H_2O, and Mg^{2+}-H_2O are −13.93, −51.55, −30.17, and −100.46 kJ·mol^{-1}, respectively. The interaction energy of Mg^{2+}-H_2O is significantly lower than those of the other interactions, indicating that water molecules exhibit a greater tendency to interact with Mg^{2+} compared to Na^+ or other ions, which is good consistent with the results obtained from MD calculations, as in Fig. 3(c).

The antifreeze mechanism of 0.5 M NaCl + 2.8 M $MgCl_2{\cdot}6H_2O$ electrolyte can be explained using Raman spectroscopy. Fig. 4a gives the Raman spectra of 0.5 M NaCl + X M $MgCl_2{\cdot}6H_2O$ (X = 0, 1.5, 2.8) electrolytes. For all samples, the peaks in the range of 2800 ~ 3800 cm^{-1} are attributed to O—H stretching vibration of water molecules [25]. For liquid water molecules, the hydrogen bonds in water molecules are constantly formed and broken. While water molecules are connected to each other by hydrogen bonds, forming an ordered lattice structure in ice [42]. In order to verify the effect of Mg^{2+} on the freezing point of the solution, Figs. 4b-d show the experimental and calculated Raman results. The observed broad peaks within 2800 ~ 3800 cm^{-1} can be categorized into three distinct components, (i) the peak around 3230 cm^{-1} corresponds to strongly hydrogen bonded water (SHW), where a water molecule is typically surrounded by four hydrogen bonds. (ii) The peak near 3620 cm^{-1} represents non-hydrogen bonded water (NHW), no hydrogen bonds exist around water molecules. (iii) The peak around 3450 cm^{-1} reflects weak hydrogen bonded water (WHW), where the number of hydrogen bonds surrounding a water molecule is intermediate between those of SHW and NHW [24,43]. Therefore, the hydrogen bonding network between water molecules can be destroyed by reducing the contents of SHW, thus effectively lowering the freezing point of the solution. For different electrolytes, the proportion of water with different hydrogen bonding states can be compared by the integrated area of the fitted peak, as shown in Fig. 4e. The SHW contents are 43.0%, 33.2%, and 25.8% for 0.5 m NaCl electrolyte, 0.5 M NaCl + 1.5 M $MgCl_2{\cdot}6H_2O$ electrolyte, and 0.5 M NaCl + 2.8 M $MgCl_2{\cdot}6H_2O$ electrolyte, respectively. It can be clearly observed that with the increase of $MgCl_2{\cdot}6H_2O$ concentration, the SHW content gradually decreases, resulting in a lower freezing point for the solution. This finding aligns closely with the results predicted by both MD and DFT calculations.

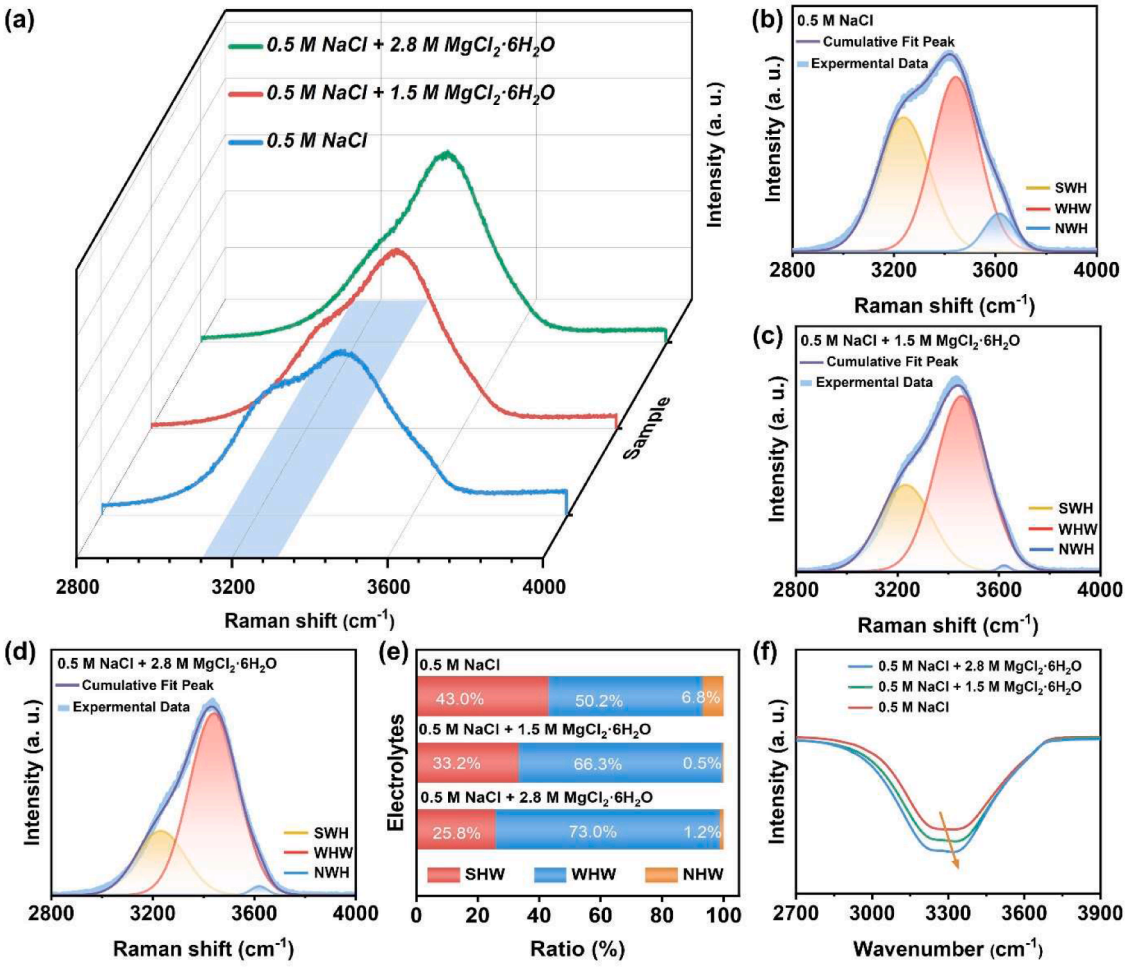

Fig. 4. (a) Raman results for various electrolytes. The experimental results and fitted Raman peaks: (b) 0.5 M NaCl electrolyte, (c) 0.5 M NaCl + 1.5 M $MgCl_2{\cdot}6H_2O$ electrolyte, (d) 0.5 M NaCl + 2.8 M $MgCl_2{\cdot}6H_2O$ electrolyte. (e) Composition proportion of hydrogen bonded water in different electrolytes. (f) FTIR spectra of different electrolytes.

Encouragingly, the content of WHW in the 0.5 M NaCl + 2.8 M $MgCl_2{\cdot}6H_2O$ solution reach 73.0%, which is much higher than those of the other solutions.

As depicted in Fig. 4f, the peak of the Fourier transform infrared (FTIR) spectra within 2800 ~ 3600 cm^{-1}, corresponding to the vibration of O—H bond [44]. With increasing of $MgCl_2{\cdot}6H_2O$ concentration, the absorption peak in the range of 2800 ~ 3600 cm^{-1} is observed to broaden and take a blue shift. This indicates a significant enhancement in the proportion of coordinated water and the reduction of the content of free water [31,45], leading to the destruction of the hydrogen bonding network and reducing the freezing point of the electrolyte, in good agreement with the results of Raman tests, as in Fig. 4a.

In order to verify the feasibility of 0.5 M NaCl + 2.8 M $MgCl_2{\cdot}6H_2O$ as electrolyte for low-temperature ASIBs, cells are constructed with $Na_2CoFe(CN)_6$ and activated carbon, and 0.5 M NaCl + 2.8 M $MgCl_2{\cdot}6H_2O$, are used as cathode, anode materials and electrolyte, respectively. The structural characterization of the electrode materials is plotted in Figs. S10-S12. As shown in Fig. S13, the cyclic voltammetry (CV) curves of $Na_2CoFe(CN)_6$ shows excellent stability and has good compatibility with the electrolyte [46]. The charge-discharge curve test of activated carbon is shown in the Fig S14. Figs. 5a and S15 show the performance of ASIBs during charging and discharging under different temperatures at a current density of 1 C, and the specific capacities are 106.1, 101.3, 92.5, 89.6, 84.5, and 74.0 mAh g^{-1} at 25, 0, −10, −20, −30, and −40 °C, respectively. Compared with the specific capacity at 25 °C, the capacity retention of ASIBs is 74.7% at −40 °C. The initial specific capacity of the battery was restored when the temperature rose from −40 °C to 25 °C, indicating that ASIBs exhibit excellent anti-frost properties and good reversibility. Meanwhile at 25 °C, the cycling performance shows a specific capacity of 81.0 mAh g^{-1} at 10 C, and the capacity retention rate is an astonishing 96.5% after 40,000 cycles, as shown in Fig. S16.

As depicted in Fig. 5b, the specific capacity of the battery at −40 °C can reach up to 74.0 mAh g^{-1} in the first cycle at 1 C. Even after 600 cycles, the battery can still provide a specific capacity of 73.4 mAh g^{-1} at 1 C, with a capacity retention of 99.2%. The rate performance of the battery is tested at −40 °C to intuitively observe the rapid charging and discharging capabilities of the battery, as shown in Fig. 5c and S17. When the current densities are 1 C, 2 C, 3 C, 4 C, 5 C, 6 C, and 10 C, the battery delivers average discharge-specific capacities of 73.9, 67.2, 62.4, 58.6, 55.1, 52.1, 42.1 mAh g^{-1}, respectively. When the current density is reduced from 10 C back to 1 C, the specific capacity can recover to the initial level, demonstrating that even under −40 °C, extremely excellent rate capabilities are exhibited by ASIBs. Moreover, ASIBs using 0.5 M NaCl + 2.8 M $MgCl_2{\cdot}6H_2O$ as electrolyte deliver superior long-term cycling stability under low-temperature conditions. After 10,000 cycles at a current density of 10 C under −40 °C, the capacity retention rate can still reach about ~ 100%, and the coulombic efficiency reaches 99.5%, as shown in Fig. 5d. These results outperform previously reported data in Fig. 5e [10,21,24,25,31,44,45,47–55]. To demonstrate practical low-temperature performance, three red LEDs, each with a power rating of 0.02 W and an excitation voltage of 1.8 V, were

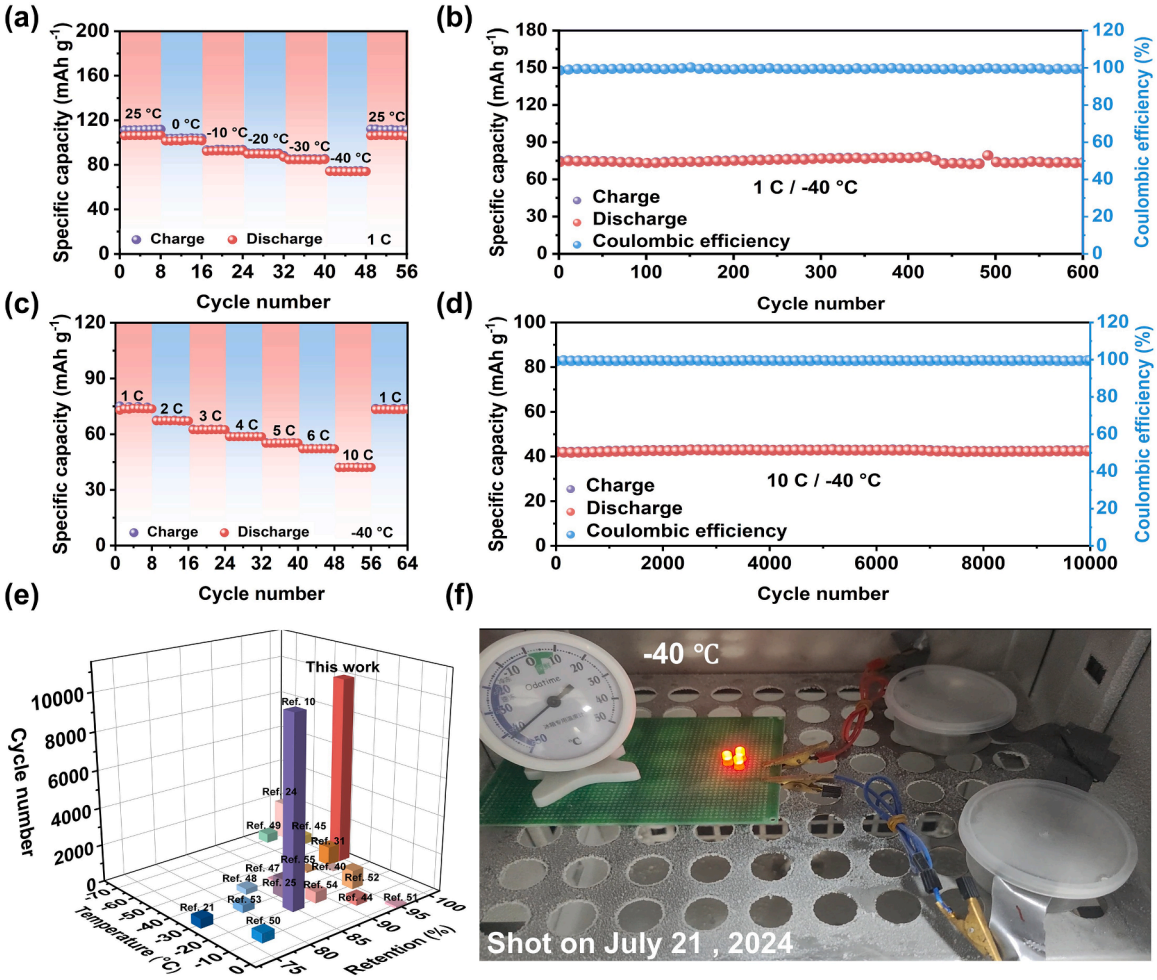

Fig. 5. The electrochemical performance of $Na_2CoFe(CN)_6$//AC battery using 0.5 M NaCl + 2.8 M $MgCl_2{\cdot}6H_2O$ electrolyte. (a) In the temperature range of 25 °C to −40 °C, the specific capacity of the battery varies at 1 C. (b) Cyclic performances of the battery at 1 C under −40 °C. (c) The electrochemical performance of the battery when tested under −40 °C with different current density. (d) Cycling performance at a high current density of 10 C under −40 °C. (e) Comparison of the cyclic stability of the battery in this work with that of low-temperature battery reported in the literature. (f) The optical image of the working battery at −40 °C.

successfully powered by two ASIBs connected in series at −40 °C, proving its feasibility in low temperature environment (Fig. 5f and Video S1).

Considering the coexistence of Na^+ and Mg^{2+} in the electrolyte, it is necessary to verify the actual identity of the carrier ions during the cycling. Firstly, 0.5 M NaCl + 2.8 M $MgCl_2{\cdot}6H_2O$ is used as the electrolyte (where Ag/AgCl and AC serves as reference and counter electrode, respectively) in the potential range of 0 ~ 1.2 V, and the $Na_2CoFe(CN)_6$ electrode is subjected to multiple charge and discharge tests. Thereafter, the electrode is exposed to an ex-situ XPS test in a state of charging to 1.2 V and discharging to 0 V. At ~ 1070.8 eV, as shown in Fig. S18, a weak Na 1 s peak is detected when measured on the $Na_2CoFe(CN)_6$ electrode under 1.2 V, which is due to the continuous extraction of Na^+ from the cathode in the charged state. A strong peak of Na 1 s can be observed at ~ 1071.9 eV at 0 V, which is because Na^+ is constantly embedded in the cathode during the discharge process. In contrast, two strong peaks of Mg^{2+} at ~ 51.4 eV and ~ 54.9 eV can be detected both during charging and discharging, respectively. The peak magnitude is almost unchanged, indicating that Mg^{2+} can be ignored during the charging and discharging of the $Na_2CoFe(CN)_6$ electrode. Therefore, Mg^{2+} only reduces the SHW content by coordinating with water molecules, while Na^+ is the ion that plays the role of charge carrier. In order to further investigate the effect of Mg^{2+} on the battery. The cycling tests are performed on the batteries with the use of 0.5 M NaCl, 2.8 M $MgCl_2{\cdot}6H_2O$ and 0.5 M NaCl + 2.8 M $MgCl_2{\cdot}6H_2O$ electrolytes, as illustrated in Figs. S19a-c. The obtained specific capacities for the two electrolyte composition cells obtained are 111.6, 66.7 and 104.4 mAh g^{-1}, respectively. The capacity of ASIBs decayed about 6.4% after the addition of 2.8 M $MgCl_2{\cdot}6H_2O$ to the electrolyte, which is acceptable. Furthermore, the electrolyte of 0.5 M NaCl + 2.8 M $MgCl_2{\cdot}6H_2O$ demonstrated enhanced cycling stability compared to NaCl alone, aligning with the results from CV tests, as in Fig. S13.

3. Conclusion

In summary, the purely inorganic NaCl/$MgCl_2{\cdot}6H_2O$ electrolyte is utilized firstly to lower the freezing point of aqueous electrolytes. At −50 °C, the 0.5 M NaCl + 2.8 M $MgCl_2{\cdot}6H_2O$ electrolyte demonstrates a significantly higher ionic conductivity (9.36 mS cm^{-1}). On the basis of theoretical calculations and characterization tests, the interaction between Mg^{2+} and water molecules has been systematically analyzed, revealing that the formation of $Mg^{2+}\cdots$O—H bond disrupts the original hydrogen bond network, thereby lowering the freezing point. Electrochemical tests and ex-XPS results confirmed that Na^+ functions as the carrier ion, while Mg^{2+} remains electrochemically inert during cycling. With the optimized electrolyte, the purely inorganic $Na_2CoFe(CN)_6$//AC battery exhibits a capacity retention of 96.5% after 40,000 cycles at 10 C under 25 °C and shows almost no capacity decay after 10,000 cycles at 10 C under −40 °C. Of particular note, the battery successfully powered an LED bulb at −40 °C, demonstrating considerable potential for

practical applications. This straightforward and effective design strategy opens a new pathway for the development of ASIBs with exceptional electrochemical performance at low temperatures.

CRediT authorship contribution statement

Gengzheng liu: Writing – original draft, Investigation, Data curation. **Huilian Hao:** Writing – review & editing, Supervision, Conceptualization. **Zefei Guo:** Conceptualization. **Jun Yang:** Investigation. **Wenzhong Shen:** Methodology, Funding acquisition.

Declaration of competing interest

The authors declare that they have no known competing financial interests or personal relationships that could have appeared to influence the work reported in this paper.

Acknowledgements

This work was financially supported by Class III Peak Discipline of Shanghai-Materials Science and Engineering (High-Energy Beam Intelligent Processing and Green Manufacturing), the project of Key Laboratory of Artificial Structures and Quantum Control (Ministry of Education), Shanghai Jiao Tong University.

Supplementary materials

Supplementary material associated with this article can be found, in the online version, at doi:10.1016/j.ensm.2025.104149.

References

[1] J. Xu, J. Zhang, T.P. Pollard, Q. Li, S. Tan, S. Hou, H. Wan, F. Chen, H. He, E. Hu, K. Xu, X.-Q. Yang, O. Borodin, C. Wang, Electrolyte design for Li-ion batteries under extreme operating conditions, Nature 614 (2023) 694–700, https://doi.org/10.1038/s41586-022-05627-8.

[2] Y. Jin, P.M.L. Le, P. Gao, Y. Xu, B. Xiao, M.H. Engelhard, X. Cao, T.D. Vo, J. Hu, L. Zhong, B.E. Matthews, R. Yi, C. Wang, X. Li, J. Liu, J.-G. Zhang, Low-solvation electrolytes for high-voltage sodium-ion batteries, Nat. Energy 7 (2022) 718–725, https://doi.org/10.1038/s41560-022-01055-0.

[3] J. Xie, Z. Liang, Y.-C. Lu, Molecular crowding electrolytes for high-voltage aqueous batteries, Nat. Mater. 19 (2020) 1006–1011, https://doi.org/10.1038/s41563-020-0667-y.

[4] L. Jiang, S. Han, Y.-C. Hu, Y. Yang, Y. Lu, Y.-C. Lu, J. Zhao, L. Chen, Y.-S. Hu, Rational design of anti-freezing electrolytes for extremely low-temperature aqueous batteries, Nat. Energy 9 (2024) 839–848, https://doi.org/10.1038/s41560-024-01527-5.

[5] Y. Yamada, J. Wang, S. Ko, E. Watanabe, A. Yamada, Advances and issues in developing salt-concentrated battery electrolytes, Nat. Energy 4 (2019) 269–280, https://doi.org/10.1038/s41560-019-0336-z.

[6] Y. Liao, W. Lin, Y. Zhang, J. Yang, Z. Li, Y. Ren, D. Wang, Y. Huang, L. Yuan, A weakly solvating ether electrolyte enables fast-charging and wide-temperature lithium-ion pouch cells, ACS Nano 18 (2024) 20762–20771, https://doi.org/10.1021/acsnano.4c06997.

[7] J. Yang, M. Wang, J. Ruan, Q. Li, J. Ding, F. Fang, F. Wang, Research progress in non-aqueous low-temperature electrolytes for sodium-based batteries, Sci. China Chem. 67 (2024) 4063–4084, https://doi.org/10.1007/s11426-024-1964-7.

[8] H. Bai, X. Zhu, H. Ao, G. He, H. Xiao, Y. Chen, Advances in sodium-ion batteries at low-temperature: challenges and strategies, J. Energy Chem. 90 (2024) 518–539, https://doi.org/10.1016/j.jechem.2023.11.004.

[9] A. Tron, S. Jeong, Y.D. Park, J. Mun, Aqueous Lithium-Ion Battery of Nano-$LiFePO_4$ with Antifreezing Agent of Ethyleneglycol for Low-Temperature Operation, ACS Sustainable Chem. Eng. 7 (2019) 14531–14538, https://doi.org/10.1021/acssuschemeng.9b02042.

[10] Q. Nian, S. Liu, J. Liu, Q. Zhang, J. Shi, C. Liu, R. Wang, Z. Tao, J. Chen, All-climate aqueous dual-ion hybrid battery with ultrahigh rate and ultralong life performance, ACS Appl. Energy Mater. 2 (2019) 4370–4378, https://doi.org/10.1021/acsaem.9b00566.

[11] M. Liu, H. Ao, Y. Jin, Z. Hou, X. Zhang, Y. Zhu, Y. Qian, Aqueous rechargeable sodium ion batteries: developments and prospects, Mater. Today Energy 17 (2020) 100432, https://doi.org/10.1016/j.mtener.2020.100432.

[12] X. Gao, J. Yang, Z. Xu, Y. Nuli, J. Wang, Recent progress of aqueous and organic/aqueous hybrid electrolytes for low-temperature rechargeable metal-ion batteries and supercapacitors, Energy Storage Mater 54 (2023) 382–402, https://doi.org/10.1016/j.ensm.2022.10.046.

[13] C. You, W. Fan, X. Xiong, H. Yang, L. Fu, T. Wang, F. Wang, Z. Zhu, J. He, Y. Wu, Design strategies for anti-freeze electrolytes in aqueous energy storage devices at low temperatures, Adv. Funct. Mater. 34 (2024) 2403616, https://doi.org/10.1002/adfm.202403616.

[14] Z. Xing, W. Zhao, B. Yu, Y. Wang, L. Zhou, P. Xiong, M. Chen, J. Zhu, Electrolyte design strategies for aqueous sodium-ion batteries: progress and prospects, Small 20 (2024) 2405442, https://doi.org/10.1002/smll.202405442.

[15] Y. Hu, R. Shi, Y. Ren, W. Peng, C. Feng, Y. Zhao, S. Zheng, W. Li, Z. Sun, J. Guo, S. Guo, X. Wang, F. Yan, A "Two-in-One" Strategy for Flexible Aqueous Batteries Operated at -80 °C, Adv. Funct. Mater. 32 (2022) 2203081, https://doi.org/10.1002/adfm.202203081.

[16] C. Ni, C. Hao, J. Tan, X. Cai, G. Ling, Q. Wu, J. Wu, X. Wang, Fabrication of $Co_{1.5}Ni_{1.5}S_4$ and Prussian blue analogues composites with yolk-shell heterostructures as cathode and biomass derived carbon as anode for asymmetric supercapacitors, J. Cleaner Prod. 466 (2024) 142844, https://doi.org/10.1016/j.jclepro.2024.142844.

[17] Q. Rong, W. Lei, J. Huang, M. Liu, Low temperature tolerant organohydrogel electrolytes for flexible solid-state supercapacitors, Adv. Energy Mater. 8 (2018) 1801967, https://doi.org/10.1002/aenm.201801967.

[18] K. Zhu, Z. Sun, Z. Li, P. Liu, X. Chen, L. Jiao, Aqueous sodium ion hybrid batteries with ultra-long cycle life at -50 °C, Energy Storage Mater 53 (2022) 523–531, https://doi.org/10.1016/j.ensm.2022.09.019.

[19] Q. Nian, J. Wang, S. Liu, T. Sun, S. Zheng, Y. Zhang, Z. Tao, J. Chen, Aqueous Batteries Operated at -50°C, Angew. Chem. Int. Ed. 58 (2019) 16994–16999, https://doi.org/10.1002/anie.201908913.

[20] Y. Sun, Y. Zhang, Z. Xu, W. Gou, X. Han, M. Liu, C.M. Li, Dilute hybrid electrolyte for low-temperature aqueous sodium-ion batteries, ChemSusChem 15 (2022) e202201362, https://doi.org/10.1002/cssc.202201362.

[21] Y. Cheng, X. Chi, J. Yang, Y. Liu, Cost attractive hydrogel electrolyte for low temperature aqueous sodium ion batteries, J. Energy Storage 40 (2021) 102701, https://doi.org/10.1016/j.est.2021.102701.

[22] H. Ao, C. Chen, Z. Hou, W. Cai, M. Liu, Y. Jin, X. Zhang, Y. Zhu, Y. Qian, Electrolyte solvation structure manipulation enables safe and stable aqueous sodium ion batteries, J. Mater. Chem. A 8 (2020) 14190–14197, https://doi.org/10.1039/D0TA04800C.

[23] Y. Zhang, J. Xu, Z. Li, Y. Wang, S. Wang, X. Dong, Y. Wang, All-climate aqueous Na-ion batteries using "water-in-salt" electrolyte, Sci. Bull. 67 (2022) 161–170, https://doi.org/10.1016/j.scib.2021.08.010.

[24] Q. Zhang, Y. Ma, Y. Lu, L. Li, F. Wan, K. Zhang, J. Chen, Modulating electrolyte structure for ultralow temperature aqueous zinc batteries, Nat. Commun. 11 (2020) 4463, https://doi.org/10.1038/s41467-020-18284-0.

[25] K. Zhu, Z. Li, Z. Sun, P. Liu, T. Jin, X. Chen, H. Li, W. Lu, L. Jiao, Inorganic electrolyte for low-temperature aqueous sodium ion batteries, Small 18 (2022) 2107662, https://doi.org/10.1002/smll.202107662.

[26] B. Zhao, H. Hao, H. Lei, J. Yang, L. Tang, X. Shi, W. Li, W. Shen, G. He, An anti-freezing pure inorganic electrolyte for long cycle life aqueous sodium-ion batteries at -40 °C, Energy Storage Mater 71 (2024) 103562, https://doi.org/10.1016/j.ensm.2024.103562.

[27] R. Hou, S. Guo, H. Zhou, Atomic insights into advances and issues in low-temperature electrolytes, Adv. Energy Mater. 13 (2023) 2300053, https://doi.org/10.1002/aenm.202300053.

[28] L. Liu, Z. Shadike, X. Cai, M. Hong, Y. Gao, S. Shen, J. Zhang, Regulating the solvation structure of an acetonitrile-based electrolyte for Li/NMC811 batteries cycled at low temperature, J. Mater. Chem. A 12 (2024) 6947–6954, https://doi.org/10.1039/D3TA07347E.

[29] D. Li, D. Zeng, X. Yin, H. Han, L. Guo, Y. Yao, Phase diagrams and thermochemical modeling of salt lake brine systems. II. NaCl+H_2O, KCl+H_2O, $MgCl_2$+H_2O and $CaCl_2$+H_2O systems, Calphad 53 (2016) 78–89, https://doi.org/10.1016/j.calphad.2016.03.007.

[30] N. Chang, T. Li, R. Li, S. Wang, Y. Yin, H. Zhang, X. Li, An aqueous hybrid electrolyte for low-temperature zinc-based energy storage devices, Energy Environ. Sci. 13 (2020) 3527–3535, https://doi.org/10.1039/D0EE01538E.

[31] M. Wang, T. Li, Y. Yin, J. Yan, H. Zhang, X. Li, A -60°C Low-temperature aqueous lithium ion-bromine battery with high power density enabled by electrolyte design, Adv. Energy Mater. 12 (2022) 2200728, https://doi.org/10.1002/aenm.202200728.

[32] W. Sun, Z. Xu, C. Qiao, B. Lv, L. Gai, X. Ji, H. Jiang, L. Liu, Antifreezing proton zwitterionic hydrogel electrolyte via ionic hopping and grotthuss transport mechanism toward solid supercapacitor working at -50°C, Adv. Sci. 9 (2022) 2201679, https://doi.org/10.1002/advs.202201679.

[33] H.-I. Kim, E. Shin, S.-H. Kim, K.M. Lee, J. Park, S.J. Kang, S. So, K.C. Roh, S. K. Kwak, S.-Y. Lee, Aqueous eutectic lithium-ion electrolytes for wide-temperature operation, Energy Storage Mater 36 (2021) 222–228, https://doi.org/10.1016/j.ensm.2020.12.024.

[34] S. Zhong, Y. Yu, Y. Yang, Y. Yao, L. Wang, S. He, Y. Yang, L. Liu, W. Sun, Y. Feng, H. Pan, X. Rui, Y. Yu, Molecular engineering on solvation structure of carbonate electrolyte toward durable sodium metal battery at -40°C, Angew. Chem. Int. Ed. 62 (2023) e202301169, https://doi.org/10.1002/anie.202301169.

[35] M. Sun, Z. Zhang, S. Fu, Y. Zhang, R. Wang, H. Mu, C. Lian, W. Wang, G. Wang, A multifunctional electrolyte additive for zinc-ion capacitors with low temperature resistant and long lifespan, J. Energy Chem. 94 (2024) 477–485, https://doi.org/10.1016/j.jechem.2024.02.060.

[36] H. Wang, T. Liu, X. Du, J. Wang, Y. Yang, H. Qiu, G. Lu, H. Li, Z. Chen, J. Zhao, G. Cui, Hybrid electrolytes enabling in-situ interphase protection and suppressed electrode dissolution for aqueous sodium-ion batteries, Batter. Supercaps 5 (2022) e202200246, https://doi.org/10.1002/batt.202200246.

[37] L. Li, H. Cheng, J. Zhang, Y. Guo, C. Sun, M. Zhou, Q. Li, Z. Ma, J. Ming, Quantitative chemistry in electrolyte solvation design for aqueous batteries, ACS Energy Lett 8 (2023) 1076–1095, https://doi.org/10.1021/acsenergylett.2c02585.
[38] H. Bi, X. Wang, H. Liu, Y. He, W. Wang, W. Deng, X. Ma, Y. Wang, W. Rao, Y. Chai, H. Ma, R. Li, J. Chen, Y. Wang, M. Xue, A Universal approach to aqueous energy storage via ultralow-cost electrolyte with super-concentrated sugar as hydrogen-bond-regulated solute, Adv. Mater. 32 (2020) 2000074, https://doi.org/10.1002/adma.202000074.
[39] Y. Shi, R. Wang, S. Bi, M. Yang, L. Liu, Z. Niu, An anti-freezing hydrogel electrolyte for flexible zinc-ion batteries operating at -70°C, Adv. Funct. Mater. 33 (2023) 2214546, https://doi.org/10.1002/adfm.202214546.
[40] N. Patil, C. De La Cruz, D. Ciurduc, A. Mavrandonakis, J. Palma, R. Marcilla, An ultrahigh performance zinc-organic battery using poly(catechol) Cathode in Zn $(TFSI)_2$-Based concentrated aqueous electrolytes, Adv. Energy Mater. 11 (2021) 2100939, https://doi.org/10.1002/aenm.202100939.
[41] T. Sun, X. Yuan, K. Wang, S. Zheng, J. Shi, Q. Zhang, W. Cai, J. Liang, Z. Tao, An ultralow-temperature aqueous zinc-ion battery, J. Mater. Chem. A 9 (2021) 7042–7047, https://doi.org/10.1039/D0TA12409E.
[42] J. Liu, C. Yang, X. Chi, B. Wen, W. Wang, Y. Liu, Water/sulfolane hybrid electrolyte achieves ultralow-temperature operation for high-voltage aqueous lithium-ion batteries, Adv. Funct. Mater. 32 (2022) 2106811, https://doi.org/10.1002/adfm.202106811.
[43] C. You, W. Wu, W. Yuan, P. Han, Q. Zhang, X. Chen, X. Yuan, L. Liu, J. Ye, L. Fu, Y. Wu, Brine refrigerants for low-cost, safe aqueous supercapacitors with ultra-long stable operation at low temperatures, Adv. Funct. Mater. 33 (2023) 2208206, https://doi.org/10.1002/adfm.202208206.
[44] S. Liu, T. Lei, Q. Song, J. Zhu, C. Zhu, High Energy, Long cycle, and superior low temperature performance aqueous na–zn hybrid batteries enabled by a low-cost and protective interphase film-forming electrolyte, ACS Appl. Mater. Interfaces 14 (2022) 11425–11434, https://doi.org/10.1021/acsami.1c23806.
[45] T. Sun, H. Du, S. Zheng, J. Shi, Z. Tao, High power and energy density aqueous proton battery operated at -90°C, Adv. Funct. Mater. 31 (2021) 2010127, https://doi.org/10.1002/adfm.202010127.
[46] C. Hao, C. Ni, X. Wang, Y. Pan, Q. Wu, J. Wu, X. Wang, Fabrication of three-dimensional CuS_2@$CoNi_2S_4$ core–shell rod-like structures as cathode and thistle-derived carbon as anode for hybrid supercapacitors, Chem. Eng. J. 465 (2023) 143024, https://doi.org/10.1016/j.cej.2023.143024.
[47] J. Chen, Y. Peng, Y. Yin, Z. Fang, Y. Cao, Y. Wang, X. Dong, Y. Xia, A desolvation-free sodium dual-ion chemistry for high power density and extremely low temperature, Angew. Chem. Int. Ed. 60 (2021) 23858–23862, https://doi.org/10.1002/anie.202110501.
[48] X. Wang, X. Yin, X. Feng, Y. Li, X. Dong, Q. Shi, Y. Zhao, J. Zhang, Rational design of $Na_{0.67}Ni_{0.2}Co_{0.2}Mn_{0.6}O_2$ microsphere cathode material for stable and low temperature sodium ion storage, Chem. Eng. J. 428 (2022) 130990, https://doi.org/10.1016/j.cej.2021.130990.
[49] F. Yue, Z. Tie, S. Deng, S. Wang, M. Yang, Z. Niu, An ultralow temperature aqueous battery with proton chemistry, Angew. Chem. Int. Ed. 60 (2021) 13882–13886, https://doi.org/10.1002/anie.202103722.
[50] D. Reber, R.-S. Kühnel, C. Battaglia, Suppressing crystallization of water-in-salt electrolytes by asymmetric anions enables low-temperature operation of high-voltage aqueous batteries, ACS Mater. Lett. 1 (2019) 44–51, https://doi.org/10.1021/acsmaterialslett.9b00043.
[51] J. Chen, J. Vatamanu, L. Xing, O. Borodin, H. Chen, X. Guan, X. Liu, K. Xu, W. Li, Improving electrochemical stability and low-temperature performance with water/acetonitrile hybrid electrolytes, Adv. Energy Mater. 10 (2020) 1902654, https://doi.org/10.1002/aenm.201902654.
[52] Z. Tang, H. Wang, P. Wu, S. Zhou, Y. Huang, R. Zhang, D. Sun, Y. Tang, H. Wang, Electrode–electrolyte interfacial chemistry modulation for ultra-high rate sodium-ion batteries, Angew. Chem. Int. Ed. 61 (2022) e202200475, https://doi.org/10.1002/anie.202200475.
[53] Z. Li, N. Yao, L. Yu, Y.-X. Yao, C.-B. Jin, Y. Yang, Y. Xiao, X.-Y. Yue, W.-L. Cai, L. Xu, P. Wu, C. Yan, Q. Zhang, Inhibiting gas generation to achieve ultralong-lifespan lithium-ion batteries at low temperatures, Matter 6 (2023) 2274–2292, https://doi.org/10.1016/j.matt.2023.04.012.
[54] X. Zheng, Z. Gu, J. Fu, H. Wang, X. Ye, L. Huang, X. Liu, X. Wu, W. Luo, Y. Huang, Knocking down the kinetic barriers towards fast-charging and low-temperature sodium metal batteries, Energy Environ. Sci. 14 (2021) 4936–4947, https://doi.org/10.1039/D1EE01404H.
[55] L. Yin, M. Wang, C. Xie, C. Yang, J. Han, Y. You, High-voltage cyclic ether-based electrolytes for low-temperature sodium-ion batteries, ACS Appl. Mater. Interfaces 15 (2023) 9517–9523, https://doi.org/10.1021/acsami.2c23008.